Article

Synergistic polarization engineering of dielectric towards low-voltage high-mobility solution-processed ultraflexible organic transistors

Check for updates

Mingxin Zhang, Xue Wang, Jing Sun, Yanhong Tong ✉, Cong Zhang, Hongyan Yu, Shanlei Guo, Xiaoli Zhao, Qingxin Tang ✉ & Yichun Liu

The emerging wearable skin-like electronics require the ultra-flexible organic transistor to operate at low voltage for electrical safety and energy efficiency and simultaneously enable high field-effect mobility to ensure the carrier migration ability and the switching speed of circuits. However, the currently reported low-voltage organic transistors generally present low mobility, originating from the trade-off between molecular polarity and surface polarity of the dielectrics. In this work, the orientation polarization of the dielectric is enhanced by introducing a flexible quaternary ammonium side chain, and the surface polarity is weakened by the shielding effect of the nonpolar methyl groups on the polar nitrogen atom. The resulting antisolvent QPSU dielectric enables the high-dielectric constant up to 18.8 and the low surface polarity with the polar component of surface energy only at 2.09 mJ/m^2. Such a synergistic polarization engineering between orientation polarization and surface polarity makes the solution-processed ultraflexible transistors present the ultralow operational voltage down to −3 V, the ultrahigh charge-carrier mobility up to 8.28 cm^2 V^{-1} s^{-1} at 1 Hz, excellent cyclic operational stability and long-term air stability. These results combined with the ultrathin thickness of transistor as low as 135 nm, the ultralight mass of 0.5 g/m^2, the conformal adherence capability on human skin and 1-μm blade edge, and the strong mechanical robustness with stable electrical properties for 30,000 bending cycles, open up an available strategy to successfully realize low-voltage high-mobility solution-processed organic transistor, and presents the potential application of QPSU dielectric for the next-generation wearable imperceptible skin-like electronics.

Ultraflexible organic field-effect transistors (OFETs) have exhibited great potential in next-generation imperceptive skin-like electronics[1–7], benefiting from the unique advantages of organic materials in lightweight, intrinsic mechanical flexibility, and low-temperature solution process[8–10]. To successfully integrate the ultraflexible organic transistor with the soft skin of the body, low-voltage operation is important for energy efficiency and safety of wearable electronics.

Two main strategies have emerged to realize the low-voltage operation of organic transistors: reducing the thickness of dielectrics and developing high-capacitance dielectrics[11,12]. The flexible organic transistors generally apply the polymer dielectrics that can be processed from solution. Because of the large free volume of the polymers, the thickness of the polymer dielectric is difficulty reduced down to less than 200 nm by regular solution-process technology[13,14]. Decreasing the thickness is often accompanied by dramatically decreased film uniformity and increased pinholes, resulting in failed operation as filed-effect transistor devices[15].

Another strategy is to use high-capacitance or high-dielectric constant (high-k) dielectrics, including inorganic nanoparticle hybrid materials[16], ion gels[17,18], and polar polymers[19]. However, the inorganic nanoparticles usually increase the surface roughness and hence lower the field-effect mobility[20].

Centre for Advanced Optoelectronic Functional Materials Research, and Key Laboratory of UV-Emitting Materials and Technology, Ministry of Education, Northeast Normal University, Changchun 130024, P. R. China. ✉e-mail: tongyh@nenu.edu.cn; tangqx@nenu.edu.cn

Ion gels present significantly decreased capacitance at low frequency and the ion motion towards the semiconductor layer, resulting in low mobility at low-frequency operation and time-dependent device degradation[21]. For the polar polymers, for example, poly(vinylidene fluoride) (PVDF, $k \sim 10.3$) and its derivatives, and polysilsesquioxane (PSQ), the increased capacitance originates from the enhanced orientation polarization either by introducing another electronegative atom, or by adding the polar side chains. However, the polar groups have been extensively reported to contribute to energetic disorder at the dielectric/semiconductor interface, resulting in low mobility, large bias hysteresis, and low atmospheric stability of electrical performance[22,23]. Therefore, it is urgent to synthesize polymer dielectrics that enable OFETs simultaneously with low operation voltage and high charge-carrier mobility.

Here, we propose a dielectric design strategy to simultaneously achieve low voltage and high mobility in organic transistor by introducing a flexible quaternary ammonium side chain in polysulfone (PSU), where the polar nitrogen atoms make the antisolvent dielectric enables a high-dielectric constant up to 18.8, and the three surrounded nonpolar methyl groups contribute to the low surface polarity with the polar component of surface energy only at $2.09 \, \text{mJ m}^{-2}$. The resulting solution-processed ultraflexible C8-BTBT transistors exhibit low operational voltage down to $-3 \, \text{V}$, ultrahigh field-effect mobility up to $8.28 \, \text{cm}^2 \, \text{V}^{-1} \, \text{s}^{-1}$ (1 Hz), highly cyclic stability, and air stability. These results open up a dielectric design strategy for low-voltage high-mobility organic transistors, and present the promising potential of QPSU dielectric in next-generation low-power portable and wearable electronics.

Results and discussion
Dielectric design for high-dielectric constant QPSU

For previously reported high-k polymer dielectrics, such as PVDF ($k \sim 10.3$) and its copolymers, the high-dielectric constant generally arises from the highpolarity and electronegativity F atom in the polymer backbone. The highly polarized surfaces of these polymer dielectrics make the OFETs suffer from the large bias hysteresis in double sweep transfer curves and low charge-carrier mobility[24]. For example, when the O=S=O polar groups were incorporated in the main chain of polyimide (PI) backbone, the dielectric capacitance can be increased from 19.3 to 32 nF/cm^2 and the operating voltage decreases from -15 to $-5 \, \text{V}$[25]. However, the O=S=O groups, with the high dipole moment of 4.5 debye (D)[26], also bring the high polarization effect and hence the low field-effect mobility as low as $4 \, \text{cm}^2 \, \text{V}^{-1} \, \text{s}^{-1}$ at 20 Hz.

Here, we proposed a dielectric design for synergistic polarization engineering of dielectric simultaneously towards low-voltage operation and high carrier mobility. As shown in Fig. 1a, by incorporating the flexible quaternary ammonium side chain into the PSU backbone, the QPSU dielectric with a high-dielectric constant and simultaneously with the low surface polarity was synthesized. PSU is a widely utilized polymer in rubber industry for nearly a century and is available at low cost and large scale[27]. The sulfone group, benzene rings, and ether oxygen bond in the backbone can improve the oxygen resistance, thermal resistance, and flexibility of the material[28]. According to density functional theory (DFT) calculations, the electrostatic surface potential (ESP) distribution in Fig. 1b reveals the efficiently separated positive and negative charges with inhomogeneous potential distribution after the addition of the polar quaternary ammonium side chains into PSU, originating from the large electronegativity of nitrogen[26]. Compared with the rather limited rotation of dipolar groups of main chain in PSU, the addition of the side chain in QPSU also dramatically enhances the rotation of dipolar groups. Therefore, the orientation polarization of the dielectric material can be enhanced for increased dielectric constant (Fig. 1c)[29]. In quaternary ammonium side chains, the N atom is surrounded by three nonpolar methyl groups, and the steric hindrance of methyl groups provides the shielding effect for the decreased surface polarity of the dielectric.

To confirm the successful incorporating the quaternary ammonium side chain into PSU polymer backbone, the chemical structure of PSU and QPSU are characterized by Fourier transform infrared spectroscopy spectra (FTIR) and ^{1}H nuclear magnetic resonance spectra (^{1}H NMR) (Fig. 1d, e). It

can be observed that the $-C_6H_6$, -O- and O=S=O groups appear at $2975 \, \text{cm}^{-1}$, $1257 \, \text{cm}^{-1}$, and $1074 \, \text{cm}^{-1}$ in both PSU and QPSU. For QPSU, the characteristic peak of the $-CH_2N(CH_3)_3$ group at $1461 \, \text{cm}^{-1}$ can be observed. In the NMR spectrum of Fig. 1e for QPSU, the peaks 1, 2, 3 correspond to $-CH_2$, $-N(CH_3)_3$ and $-C(CH_3)_2$, respectively. These results confirm the successful synthesis of side chain on the PSU backbone[30].

Figure 1f shows the calculated dielectric constant values of PSU and QPSU according to the equation of the dielectric thickness and the dielectric capacitance (Supplementary Fig. 1) extracted at quasi-static of 1 Hz. The capacitance measurements were carried out based on the metal-insulator-metal structure as shown in the inset of Fig. 1f. Directional polarization generally occurs when a permanent dipole moment exists in the polymeric material and reorients upon the application of an electric field. Therefore, our dielectric design incorporates molecular dipole segments of quaternary ammonium side chain, allowing for reorientation when subjected to an electric field. This results in QPSU dielectric with a high capacitance of 185 nF/cm^2 and a high-dielectric constant of 18.8 at 1 Hz. The capacitance value decreases with increasing frequency, as expected, because the orientation polarization is unable to keep up with rapid frequency changes, especially at high frequencies[31]. This phenomenon has been reported in many high-k polymer dielectrics[32]. For comparison, the dielectric constant values of the commonly used dielectrics for solution-processed flexible organic transistors, including polyimide (PI), polyethylene terephthalate (PET), poly (4-vinylphenol) (c-PVP) and poly (vinyl alcohol) (PVA/c-PVA), are also given in Fig. 1f. After incorporating the polar side chain in PSU, the dielectric constant of the dielectric increases from 3.9 to 18.8, which is much higher than the conmmonly used polymer dielectrics.

Solvent resistance of QPSU dielectric

The solvent resistance of polymer dielectric is the key to fabricate low-cost large-scale solution-processed organic transistors. Until now, lack of the available antisolvent polymer dielectrics has seriously hold back the development of the solution-processed organic transistors. In our experiments, PSU is used as the precursor material for the fabrication of the QPSU dielectric because of the strong antisolvent capability, good humidity, and temperature stability.

In order to show the promising potential of QPSU as dielectric of OFETs, the QPSU films were respectively dipped into water, acetone and chlorobenzene, and then were taken out for measurements of AFM images and mass. For comparison, PSU, and the commonly used dielectrics for flexible OFETs including PVA, PS and PDMS, were also measured. Figure 2a schematically shows the dipping process of the dielectric films into the solution, and gives the photos of the films before and after dipping. Figure 2b is the measured AFM results and Fig. 2c gives the mass change. It can be observed that the commonly used polymer dielectrics including PVA, PS and PDMS, either are dissolved by water or organic solvents, or swell, resulting in the obviously changed surface morphology and mass. The dramatically increased roughness of the PVA dielectric film in water shows the water-soluble characteristic of PVA, which has been well known to significantly affect the transistor stability, particularly, in high atmospheric humidity[33]. The dramatically increased roughness of PS and PDMS films in organic solvent makes them challenging for fabrication of solution-processed organic transistors. In contrast, both PSU and QPSU show excellent chemical resistance. PSU only can be dissolved in aprotic solvents, such as N-methylpyrrolidone (NMP) and N,N-dimethylformamide (DMF)[34], and can form orthogonal solvent system with most organic solvents. Similar to PSU, QPSU shows the excellent chemical resistance with the unchanged surface morphology and mass after dipping into water, acetone, and chlorobenzene, which makes it a good dielectric candidate for cost-efficient solution-processed organic transistors.

Further, we also investigate the insulator stability, humidity stability, thermal stability, and the mechanical stability by the dielectric constant value of QPSU dielectric. QPSU shows excellent insulating properties, with a current density of $2.6 \times 10^{-9} \, \text{A/cm}^2$ at 1 MV (Supplementary Fig. 2), which is comparable to that of reported polymer dielectrics and lower than the
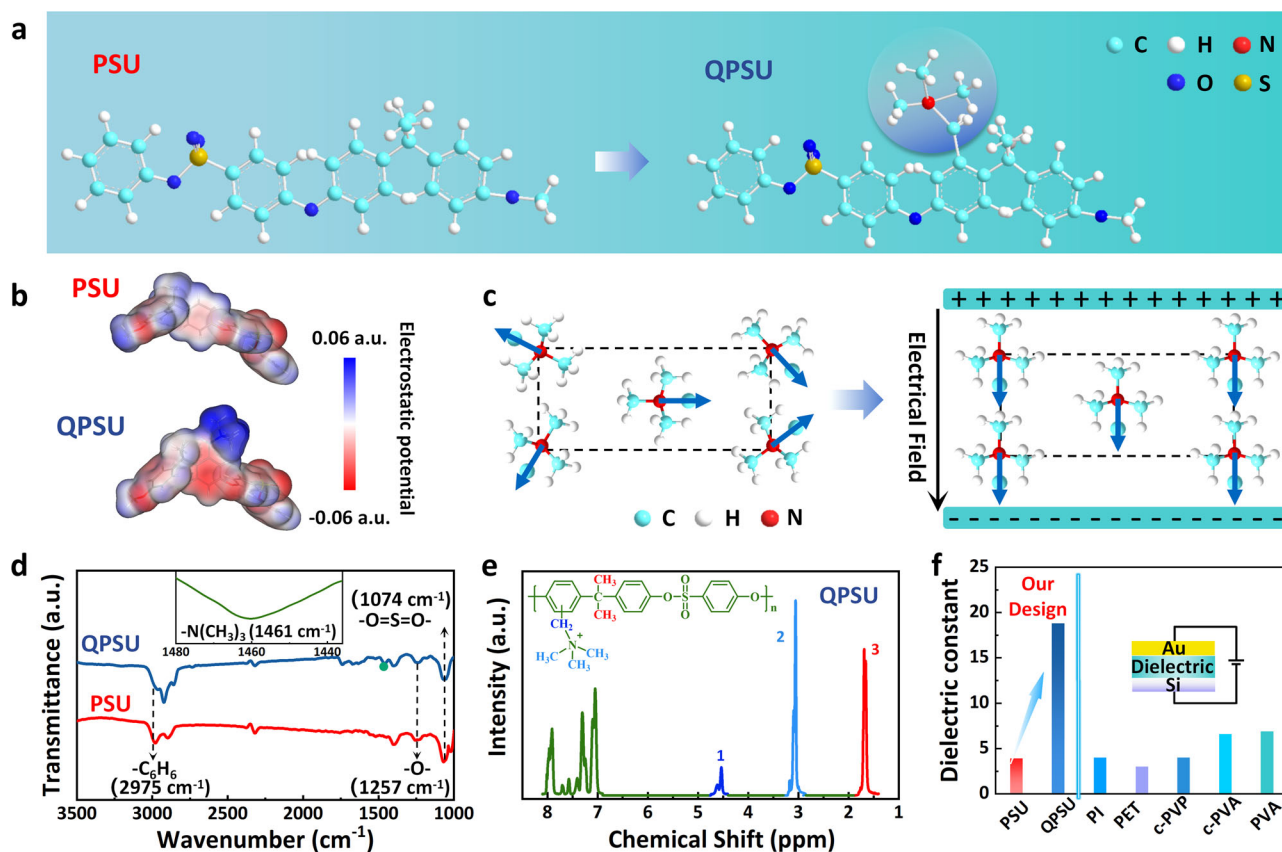
Fig. 1 | Schematic illustration of dielectric design for high-dielectric constant QPSU dielectric. a Chemical structure. **b** Electrostatic surface potential (ESP) distribution of PSU and QPSU. **c** Mechanism of orientation polarization of side chain. **d**, **e** FTIR and ^{1}H NMR spectra. **f** Dielectric constant of PSU, QPSU, and the commonly used polymer dielectrics at 1 Hz.

mostly reported low-voltage OFETs based on PAA dielectrics (Supplementary Table 1). As shown in Fig. 2d, QPSU always remain the unchanged dielectric constant value when the humidity changes from 20% to 100%, or the temperatures changes from 20 to 200 °C as the initial decomposition temperature of QPSU ($T_{5\%}$, defined as the temperature at which 5% of weight loss occurs) (Supplementary Fig. 3) is approximately at 200 °C. After 10,000 bending cycles (bending radius is 3 mm, Supplementary Fig. 4), the dielectric constant of QPSU dielectric shows negligible changes (Fig. 2e), which benefits from the good flexibility of QPSU dielectric as the Young's modulus is only 726 MPa (Supplementary Fig. 5). The stable dielectric properties of QPSU, including insulation, humidity, temperature, and mechanical stability, demonstrate its promising advantage as a dielectric for the stable operation OFETs.

Low-voltage solution-processed ultraflexible OFETs based on QPSU dielectric

To further show the advantages of QPSU as the dielectric of OFETs, the ultraflexible QPSU dielectric 8×8 transistor array is fabricated based on a solution process. As shown in Fig. 3a, poly(3,4-ethylenedioxythiophene):poly(styrenesulfonate) (PEDOT:PSS), QPSU, 2,7-dioctyl[1] benzothieno[3,2-b][1]benzothiophene (C8-BTBT), were spin-coated on the OTS modified Si wafer and serve as gate electrode, dielectric, and semiconductor layer, respectively. After that, Au was deposited and functions as source and drain electrodes. The OFET array was easily peeled off from the OTS/Si substrate with the help of the 3 M tapes as shown in Supplementary Fig. 6. The thickness of the obtained ultraflexible OFET array can be as low as 135 nm (see AFM height image in the upper right of Fig. 3a), which is in the thinnest class of the reported conformal solution-processed organic transistor as shown in Supplementary Table 2. And the array exhibits the extremely light mass of 0.5 g/m². This value is approximately one magnitude

lower than that a damselfly wing (~ 4.7 g/m², Supplementary Fig. 7), which represents the lightest reported mass for OFETs (Supplementary Table 3), so that an 8×8 array can be easily sustained by a hair, as shown in Fig. 3b. Figure 3c shows the typical photographs of a QPSU dielectric OFET array, that the length and width of the source and drain electrode are 100 μm and 3500 μm, respectively.

The transfer curves of the QPSU dielectric OFET are shown in Fig. 3d. For comparison, PSU as the QPSU precursor, and PVA as the mostly used flexible dielectric for solution-processed organic transistors, were also used as the dielectrics in OFETs with the same dielectric thickness (~ 90 nm) (Supplementary Fig. 8), and the transfer curves are given in Fig. 3d. Obviously, PSU and PVA dielectrics OFETs exhibits much higher off state current than QPSU. Due to our dielectric design, which involves the shield effect of the methyl groups surrounding the polar N atom and results in low surface polarity of the QPSU dielectric, the double sweep transfer curves of the QPSU dielectric OFET display almost no hysteresis loop as the voltage is swept between the forward and reverse directions (Supplementary Fig. 9). Figure 3e shows the color mapping of the corresponding distribution of the threshold voltage of the QPSU dielectric OFET array, and Fig. 3f is the histogram distribution of threshold voltage and operation voltage of QPSU, PSU and PVA dielectric OFETs. All the transfer curves show the ideal p-type behavior, well-defined saturation and linear regimes. The QPSU dielectric OFET array shows the good yield ratio as high as 100% and the low threshold voltage of -2 ~ -1 V, which indicates that only the low gate voltage is required to attract charges at semiconductor/dielectric interface for the formation of the conductive channel. Figure 3f shows the far lower threshold voltage and operational voltage of the QPSU dielectric device compared to that of the PSU and PVA dielectric devices. The operational voltage of the PSU and PVA dielectric OFETs is ~-40 and -60 V, respectively, when the on-state current is over 10^{-4} A. In contrast, the operational voltage of the
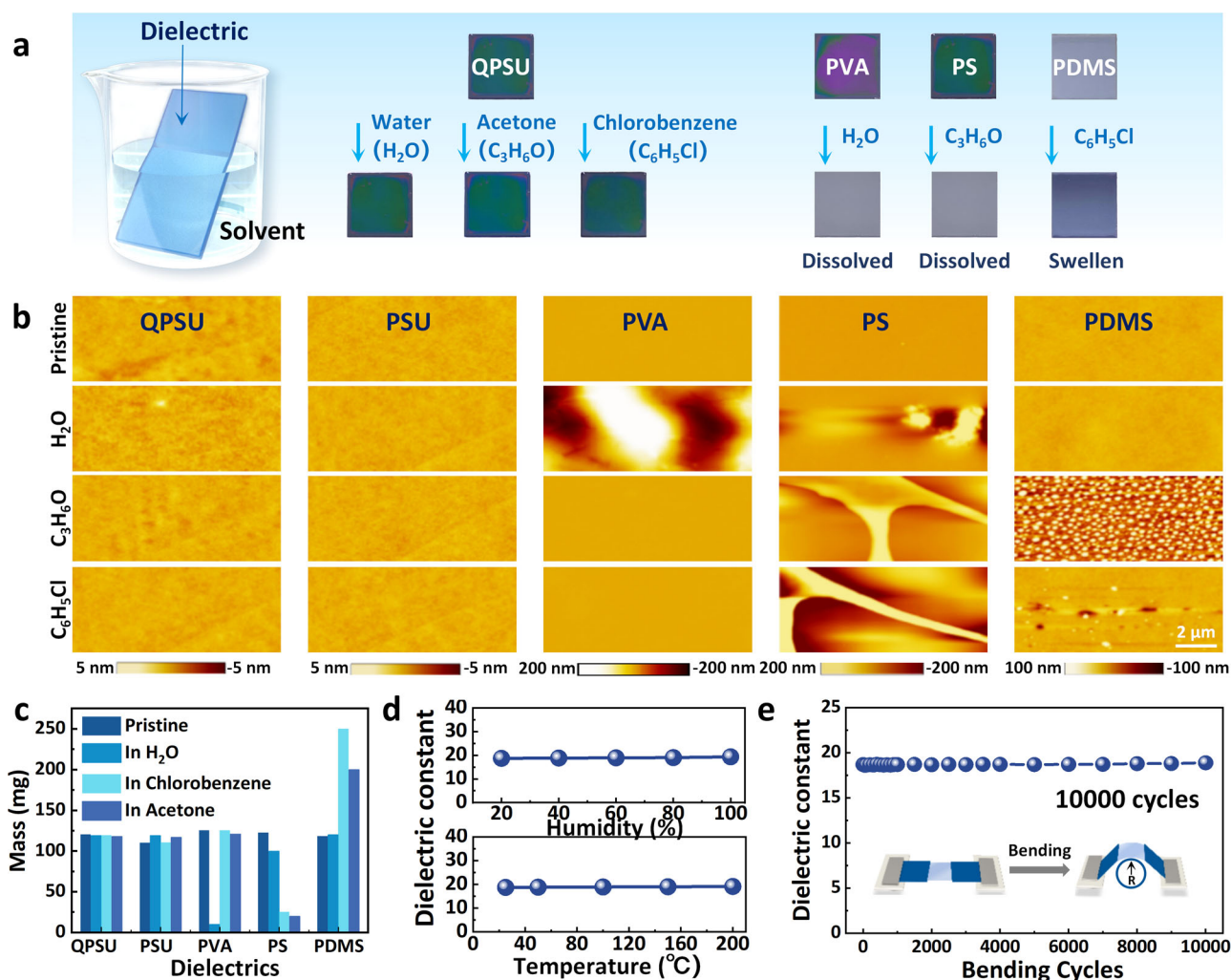
Fig. 2 | Solvent resistance and high stability of QPSU. a–c Photographs, AFM images, and mass changes of dielectrics after dipping in H_2O, acetone, and chlorobenzene, respectively. The corresponding results for PSU, PVA, PS, and PDMS dielectrics are also shown. **d** Dielectric constant of QPSU dielectric at 20~100% humidity and at the temperature of 25~200 °C. **e** Dielectric constant of QPSU dielectric during 10,000 bending cycles.

QPSU dielectric device is only at -3 ~ -4 V. Supplementary Fig. 10 illustrates the typical output curves of QPSU dielectric OFETs. The output curves exhibit the clear transition from liner to saturation regimes, as well as apparent linearity at low drain-source voltage (V_{DS}). These features are emblematic for the efficient contact injection and low contact resistance of electrode/channel layers[7]. These results confirm that the addition of the quaternary ammonium side chain in PSU is favorable for the increased dielectric constant and hence the decreased operational voltage.

As mentioned above, next-generation imperceptible skin-like electronics will need ultraflexible organic devices with low operational voltage for human safety, low-power consumption, and long-term power supply. It is desirable that OFETs are driven at the voltage lower than the normal working voltage of lithium batteries (4.5 V) that can use the daily portable power sources[35]. Figure 3g summarizes the dielectric constant values and operational voltage of the reported polymer dielectric OFETs[36–48]. Most of previous OFETs apply the low dielectric constant dielectrics and present the high operational voltage higher than 4.5 V. Very recently, Bao et al.[48] have applied a high-dielectric constant tri-layer of nitrile-butadiene rubber ($k = 28$)/poly(styrene-ethylene-butylene-styrene)/octadecyltrimethoxysilane (NBR/SEBS/OTS) to achieve an operational voltage of the transistor as low as -3 V. Obviously, compared with most previously reported solution-processed dielectrics, our QPSU dielectric shows notably high-dielectric constant of 18.8, which allows more charges to be induced at lower voltage and hence increases the drive capability of the transistors. The

operational voltage of our QPSU dielectric OFET can be work as low as -3 V. All the above results confirm the feasibility of our dielectric design via modification of quaternary ammonium side chain to achieve high-dielectric constant dielectric for next-generation battery powered low-voltage wearable and portable electronics.

High-mobility QPSU dielectric OFETs
Gate dielectrics not only should have the high-dielectric constant to allow the low-voltage operation, but also at the same time should be favorable for high field-effect mobility to achieve the key applications of OFETs in display drivers, logic circuits, amplification circuits, etc[49,50]. Typically, High-polarity dielectrics typically result in the dipole disordering, which can reduce the carrier mobility of OFETs. The presence of random dipoles at the semiconductor/ dielectric interface broadens the density of states (DOS) and leads to an increased number of tail states that hinder the transfer of charges. This can be attributed to dipole polarization, which localizes mobile charges during transportation. Richards et al. presented an analytical model to investigate the interaction between charges and the dielectric environment[51]. They calculated the broadening of the DOS as a function of the distance from the surface and discovered that the impact of dipole polarization on mobile charges was most pronounced when considering the nearest dipoles. Consequently, the dipolar disorder effect in high-polarity dielectrics results in reduced mobility, rendering them unsuitable for high-performance OFETs. Figure 4a is the color map of the charge-carrier mobility of 8×8
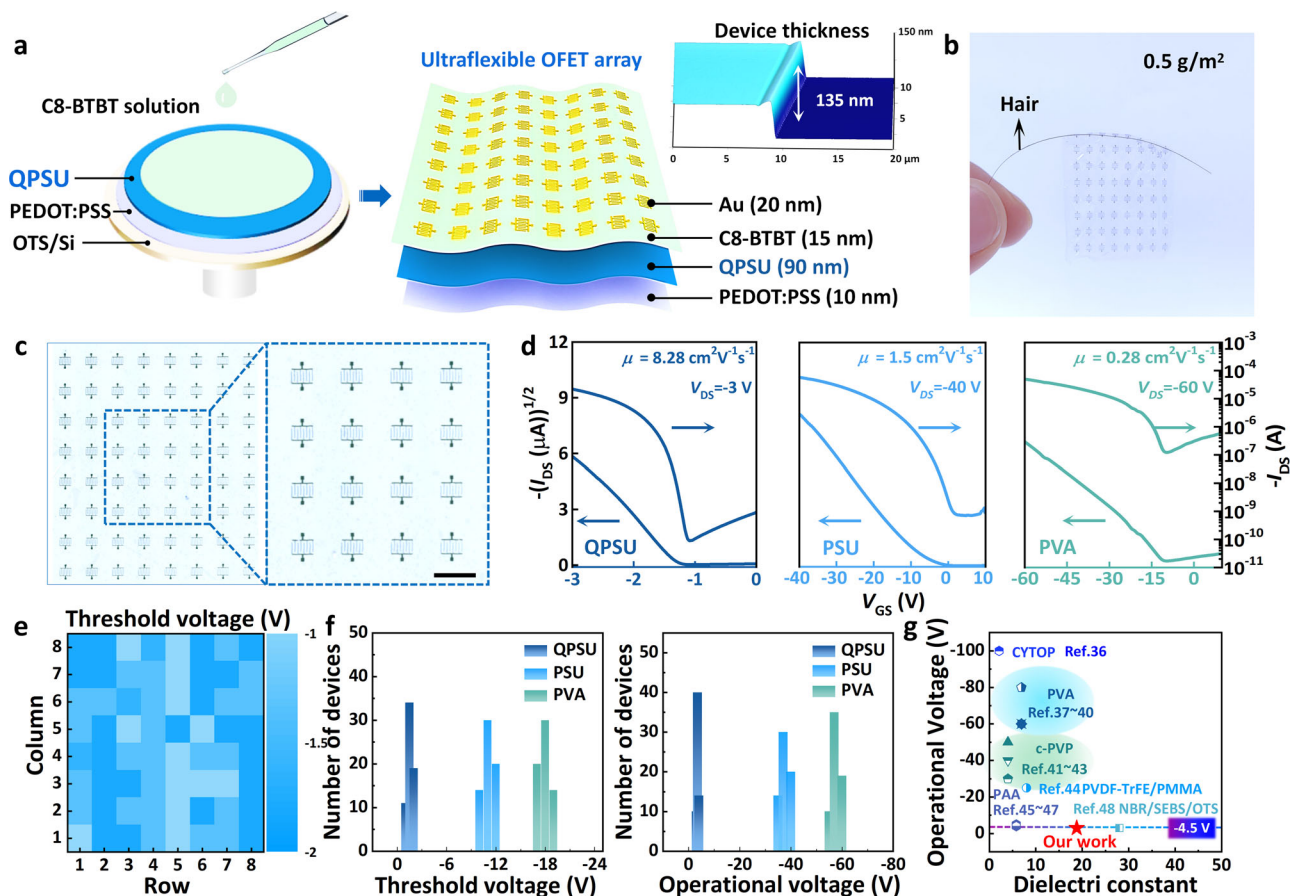
Fig. 3 | Low-voltage, high-mobility solution-processed ultraflexible C8-BTBT array based on QPSU dielectric. a Fabrication schematic and AFM height images of transistors. **b** Photograph of the transistor array sustained by a hair. **c** Photograph of 8 × 8 transistor array and magnified optical microscopy image (scale bar: 2 mm). **d** Transfer curves of transistors based on QPSU, PSU, and PVA dielectrics. **e, f** Threshold voltage color map histogram distribution of threshold voltage and operation voltage of QPSU, PSU, and PVA dielectric transistors. **g** Statistical results of the reported dielectric constant and operational voltage of solution-processed polymer dielectric OFETs.

OFET array with QPSU dielectric, and the statistical histogram of mobility distribution, with the frequency at 1 Hz. Obviously, the OFET array shows 100% fabrication success rate and high charge-carrier performance. The highest mobility is up to 8.28 $cm^2V^{-1}s^{-1}$ when the capacitance is extracted at quasi-static conditions of 1 Hz. The QPSU dielectric OFET array also exhibits the high uniformity, with the average mobility up to 5.05 $cm^2V^{-1}s^{-1}$ and a low standard deviation of 1.32 $cm^2V^{-1}s^{-1}$. For our previous work[33], which was based on the crosslinking reaction of polyethyleneimine (PEI) and epoxy resins (EP) and was named as PEI-EP dielectric by solution-processed C8-BTBT flexible organic transistor, shows a high mobility of up to 7.98 $cm^2V^{-1}s^{-1}$ when the capacitance is extracted at 1 Hz. However, the high operational voltage is as high as -60 V, which is much higher than the human safety voltage (36 V), making it unsuitable for skin-like wearable electronics and energy consumption for power supply. Furthermore, the highly crosslinked network thin film, leading to its high Young's modulus of 4.87 GPa, easily breaks in our experiments. As far as we know, this high mobility represents one of the best results of C8-BTBT OFETs with the dielectric capacitance at quasi-static condition to date as shown in Supplementary Fig. 11. The mobility extracted from a low-frequency capacitance is crucial. Bao's group[52] has reported that the high-frequency capacitance can result in overestimation of the field-effect mobility by orders of magnitude. Huang's group[53] also reported the similar results. Some mobiles such as hydrogen ions will contribute to slow polarization of the dielectric, resulting in lower capacitance value of the dielectric at the typical measured frequencies of $\geq 10^3$ Hz compared with that of low frequencies. Considering that the transistor measurements are usually carried out at quasi-static conditions (<10 Hz), using the high-

frequency capacitance will be significantly overestimated of the filed-effect mobility.

Here, the capacitance of the QPSU dielectric is measured at 1 Hz, which ensures the high-reliability mobility result. Our ultrathin QPSU dielectric transistor with the thickness of only 135 nm, shows the charge-carrier mobility two orders of magnitude higher than the previously reported thinnest transistor (150 nm, 0.098 $cm^2V^{-1}s^{-1}$)[45]. Compared with the previously reported low-voltage polymer dielectric C8-BTBT OFETs, the OFETs based on QPSU dielectric shows the lowest operational voltage and highest charge-carrier mobility (Supplementary Table 4)[54–57]. The previously reported high solution-processed transistors usually applied self-assembled monolayers (SAMs) of dielectrics or semiconductor modification to improve the crystallinity of semiconductor layers, resulting in high-mobility OFETs. For example, Ong et al. applied the silylating agents with long alkyl chain and pheyl or medium alkyl chain hybrid self-assembled monolayers (SAMs) to study the electrical performance of OFET. By modification the SiO_2 with "hybrid" dual-silane SAMs, the upper DPP-DPP semiconductor layer with high crystallinity, enabling both high mobility and on/off ratio, together with desirable transistor property[58]. In addition, the same group reported a D-A polymer semiconductor with a polymer-matrix-mediated molecular structure using polyacrylonitrile (PAN), resulting in the formation of a polymer thin film with continuous, highly ordered, and percolated semiconductor transport channels. The solution-processed polymer semiconductor OFETs exhibited extremely high mobility, reaching values as high as 16 $cm^2V^{-1}s^{-1}$, and a current on/off ratio exceeding 10^8. The mobility is an order of magnitude improvement compared to devices without the PAN semiconductor layer[59]. Compared with
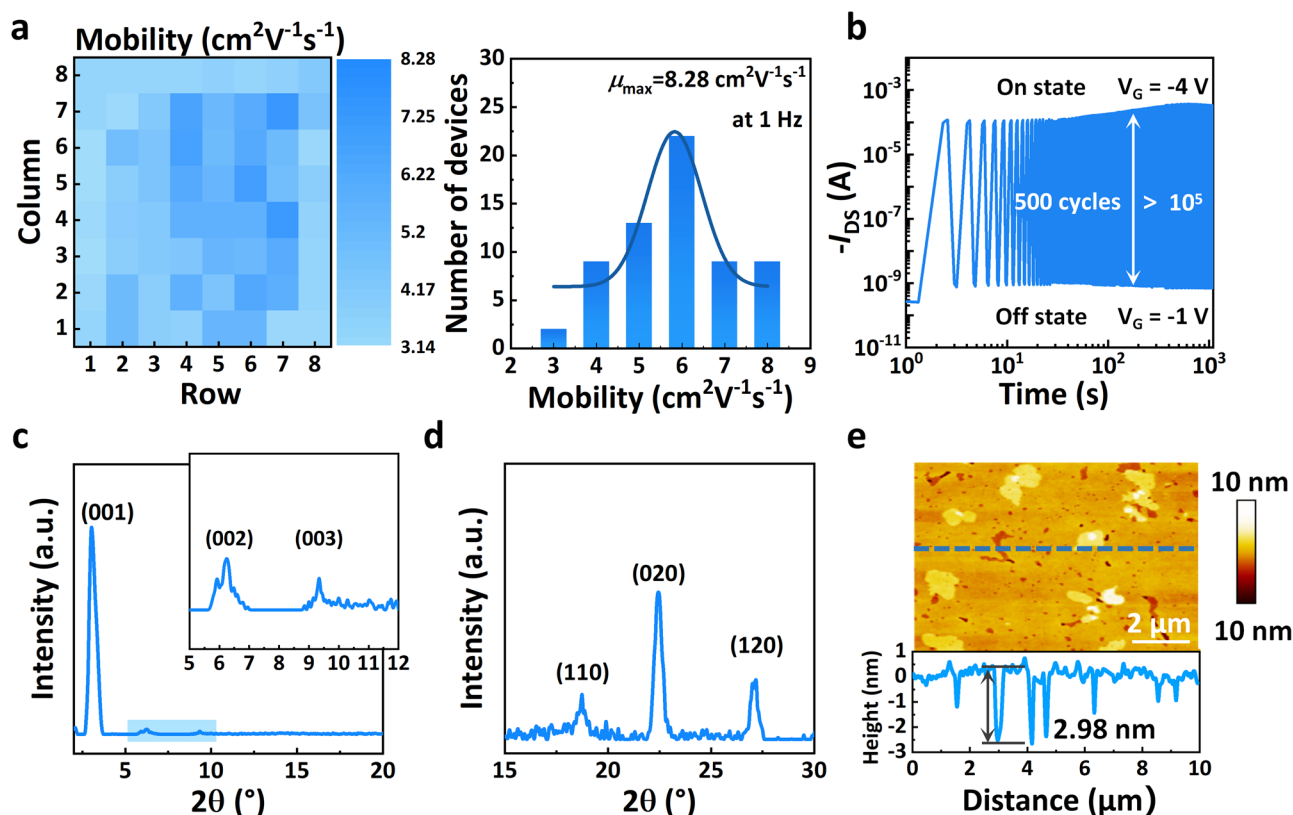
Fig. 4 | High-mobility and highly stable C8-BTBT OFET array based on QPSU dielectric. a Mobility color map and statistical histogram of mobility distribution. **b** Cycle stability for 1000 s. **c, d** Out-of-plane and in-plane GIXRD patterns of the C8-BTBT film deposited on QPSU dielectric. **e** AFM image and height curve of the C8-BTBT film on QPSU.

the high-mobility solution-processed OFETs mentioned above, our low surface polarity QPSU dielectric OFETs achieve a high mobility up to 8.28 $cm^2V^{-1}s^{-1}$ via simple direct spin-coating of the C8-BTBT film, without any complex dielectric or semiconductor modification. The mobility of the QPSU dielectric OFET is also higher than the benchmark amorphous silicon, α-Si (0.5 ~ 1.0 $cm^2V^{-1}s^{-1}$), which is sufficient for the applications such as active-matrix organic light-emitting-diode, sensors, and amplification circuits[60].

In addition, the QPSU dielectric transistors present the excellent operational stability and time stability. As shown in Fig. 4b, the device can be switched between on and off state for over 500 cycles with the on/off ratios of >10^5 indicating the good switching performance and the capability to resist disturbance[61]. The OFETs based on QPSU dielectric demonstrate remarkable bias-stress stability, as shown in Supplementary Fig. 12. With the continuous cycle test of 500 cycles (V_{DS} = -3 V and V_{GS} = 0 ~ -3 V) within 500 min, the transfer curves exhibit negligible changes. The device without packaging also shows the fairly stable electrical properties in atmospheric environment (25 °C, RH ≈ 25%). As shown in Supplementary Fig. 13, the device only shows the weak change of the mobility and threshold voltage in 120 days. All these results confirm our dielectric design via incorporating a quaternary ammonium side chain modification of PSU is a promising strategy for high-performance OFETs. As shown in Fig. 1f **and** Fig. 3, the low-voltage operation is achieved by incorporating a polar side chain onto the backbone of PSU to increase the dielectric constant. To further to investigate the crystal arrangement of C8-BTBT film deposited on QPSU dielectric, the grazing incidence X-ray diffraction (GIXRD) was performed, as shown in Fig. 4c, d. In the out-of-plane XRD patterns shown in Fig. 4c, three sharp characteristic peaks of (001), (002), and (003) existed, suggesting the well-ordered crystal structure within the C8-BTBT film. According to the equation of Bragg's Law, $2dsin\theta = n\lambda$, the calculated d-spacing from the (001) peak of the C8-BTBT film is about 2.9 nm, which is coincide with the length of the C8-BTBT molecule[62]. indicating the molecules adopt an edge-on arrangement, consistent with previous reports[63]. In the in-plane XRD patterns (Fig. 4d), the existence of (110), (020), and (120) peaks indicates the herringbone packing of the C8-BTBT molecules within the plane on the dielectric layer, which can facilitate 2D carrier transport in the semi-conductor layer[64]. In Fig. 4e, the surface morphology of the C8-BTBT film on QPSU dielectric illustrates the large crystalline size of the C8-BTBT film with the molecular step of only ~2.98 nm[65], that is coincide with the above GIXRD results, which is favorable for the decreased traps, efficient carrier transport, and high field-effect mobility[66].

Synergistic polarization engineering of QPSU dielectric

To further confirm the synergistic polarization design strategy of the QPSU dielectric to realize low-voltage operation while simultaneously achieve high mobility, we synthesized a series of dielectric molecules with different number of methyl groups on the side chains of PSU, and their dielectric properties and transistor performance are compared. The molecules with the N atom on the side chain surrounded by 0~3 methyl groups are namely Me$_0$PSU, Me$_1$PSU, Me$_2$PSU, and Me$_3$PSU (QPSU), respectively (Supplementary Methods, Supplementary Fig. 14). Figure 5a illustrates the transistor configuration, the chemical structure of the four dielectrics, and the ESP distribution of the side chains with different numbers of methyl groups by density functional theory (DFT). The surface morphologies of the four dielectrics are shown by AFM images in Supplementary Fig. 15. All the films exhibit a smooth surface with low surface roughness at 0.27~0.32 nm.

It is clear that the minima and maxima of ESP are located on H atoms by blue color and N atom by red color. For the side chain of Me$_0$PSU, the N atoms are surrounded by 3-H atoms, showing the uneven potential distribution and the strong polarization. With the increased number of methyl groups, the increased white color regions reveal the weakened potential distribution due to the poor electron-rich property of methyl group.
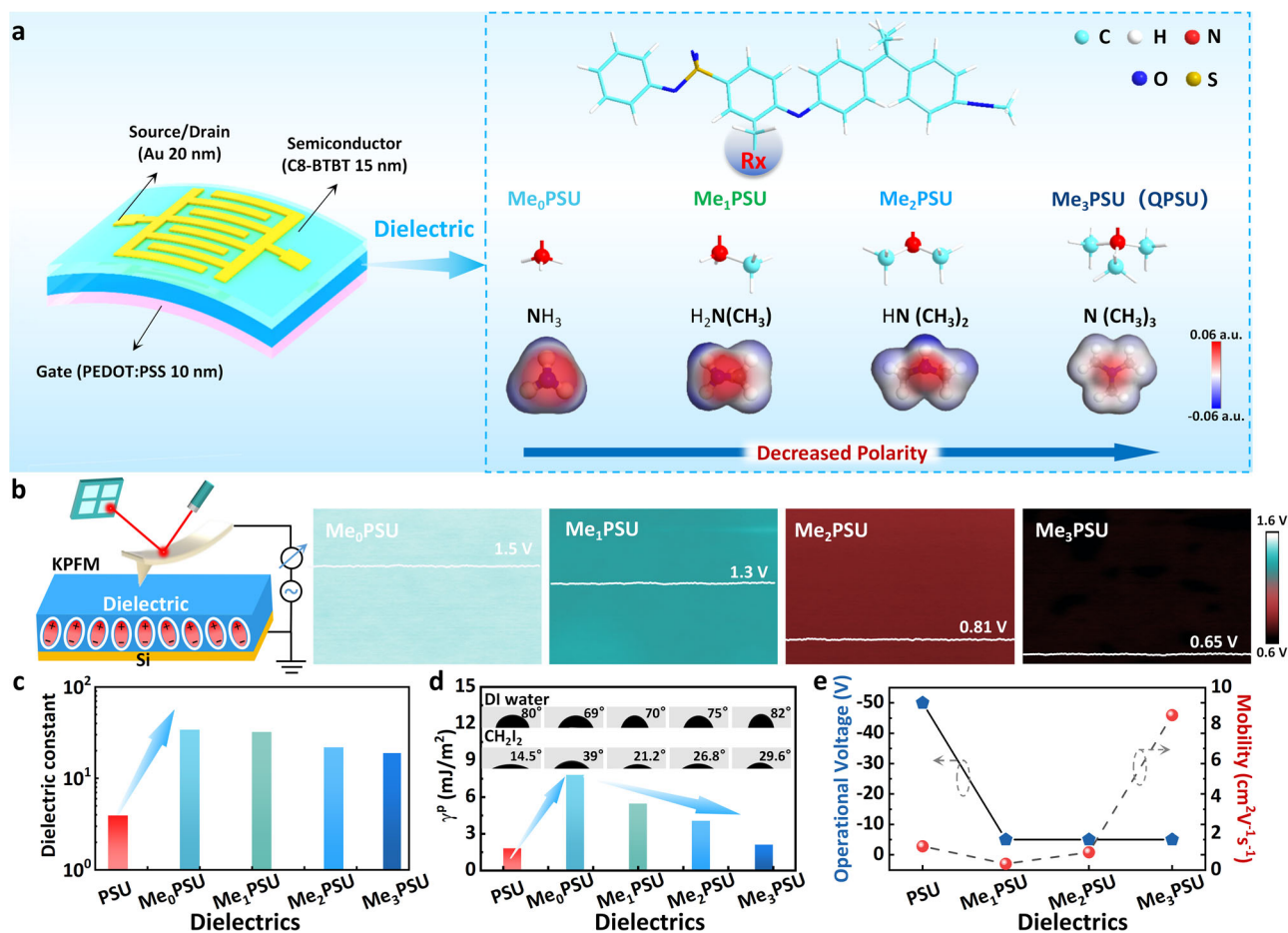
Fig. 5 | Design principle of QPSU dielectric for low-voltage operation and high carrier mobility. PSU, and the dielectrics with changed methyl group number, which are named Me$_0$PSU, Me$_1$PSU, Me$_2$PSU, and Me$_3$PSU, are compared. **a** Device structure, chemical structure, and electrostatic surface potential (ESP). **b** Surface potential measured by Kelvin probe force microscopy (KPFM). **c, d** Dielectric constant and polar components of surface energy. Insets show the tested contact angles for calculation of surface energy. **e** Operational voltage and mobility values.

Furthermore, when the 3 H end atoms are substituted by three methyl groups, the peripheral region of N atom is almost neutral characterized by white color, indicating the even potential distribution and the shielding effect of methyl groups on the surface polarity of the molecules.

Kelvin probe force microscopy (KPFM) is an effective way to show the nanometer-scale imaging of the surface potential on a wide range of polar materials. Here, as shown in KPFM images of Fig. 5b, the surface potential of the dielectrics decreases with the increased number of methyl groups on the N-based side chains[67]. In Fig. 5c, d, the dielectric constant was measured, and the polar components of surface energy (γ^p) were extracted from the measured contact angles for different PSU-based dielectric materials, respectively. It can be observed that the addition of the side chain into PSU dramatically increases the dielectric constant value (Supplementary Fig. 16) while also obviously increasing the surface polarity as shown by the increased polar component of surface energy (from PSU to Me$_3$PSU)[68]. Therefore, the incorporation of the polar side chain is favorable for the decreased operational voltage but has a negative effect on the mobility, as shown in Fig. 5e (from PSU to Me$_2$PSU, Me$_0$PSU is dissolvable and hence its solution-processed transistor is not available).

Further, with the increased methyl groups on the N-based side chain, the enhanced shielding effect of the methyl groups weakens γ^p value (Fig. 5d), resulting in the decreased surface potential as shown in Fig. 5b. It has been reported that the γ^p value suggests the surface polarity strength that has been well known to affect the mobility. Therefore, the decreased γ^p value with the increased methyl groups (Fig. 5d, from Me$_0$PSU to Me$_3$PSU) is favorable for improved mobility. As a result, the mobility presents a dramatic increase with the increased methyl groups, as shown in Fig. 5e and Supplementary Fig. 17. The polar component of the surface energy of Me$_3$PSU is only 2.09 mJ m^{-2}, which is even lower than the nonpolar poly(methylmethacrylate) (PMMA) dielectric of 2.31 mJ m^{-2} (Supplementary Table 5). Therefore, our QPSU dielectric device presents mobility as high as 8.28 cm^2 V^{-1} s^{-1}. These results powerfully confirm the feasibility of our dielectric design for synergistic polarization engineering simultaneously towards low-voltage operation and high carrier mobility of solution-processed organic transistors.

Conformal OFETs based on QPSU dielectric

To show the promising application potential of our QPSU dielectric OFETs in skin-like portable and wearable electronics, the ultraflexible devices were adhered on the human arm by van der Waals forces without any additional adhesives, and a series of tests of the mechanical flexibility were performed, as shown in Fig. 6a. When the skin is compressed, pressed, stretched and twisted, the transistors always remain conformal deformation with the moving of skin without any mechanical cracks or visible damage. Even though the above process was repeated 30 times, the transfer curves remain consistent without any decrease in electrical performance (Supplementary Fig. 18). Figure 6b shows the wafer-scale fabrication of the QPSU dielectric transistors by photolithography. Photolithography, as the staple technique in the silicon-based industry, has successfully enabled shrinking of the channel length, allowing highly integrated circuit fabrication. Unfortunately, the conventional photolithography is difficultly compatible with polymer dielectrics, originating from lacking of the polymer dielectrics with
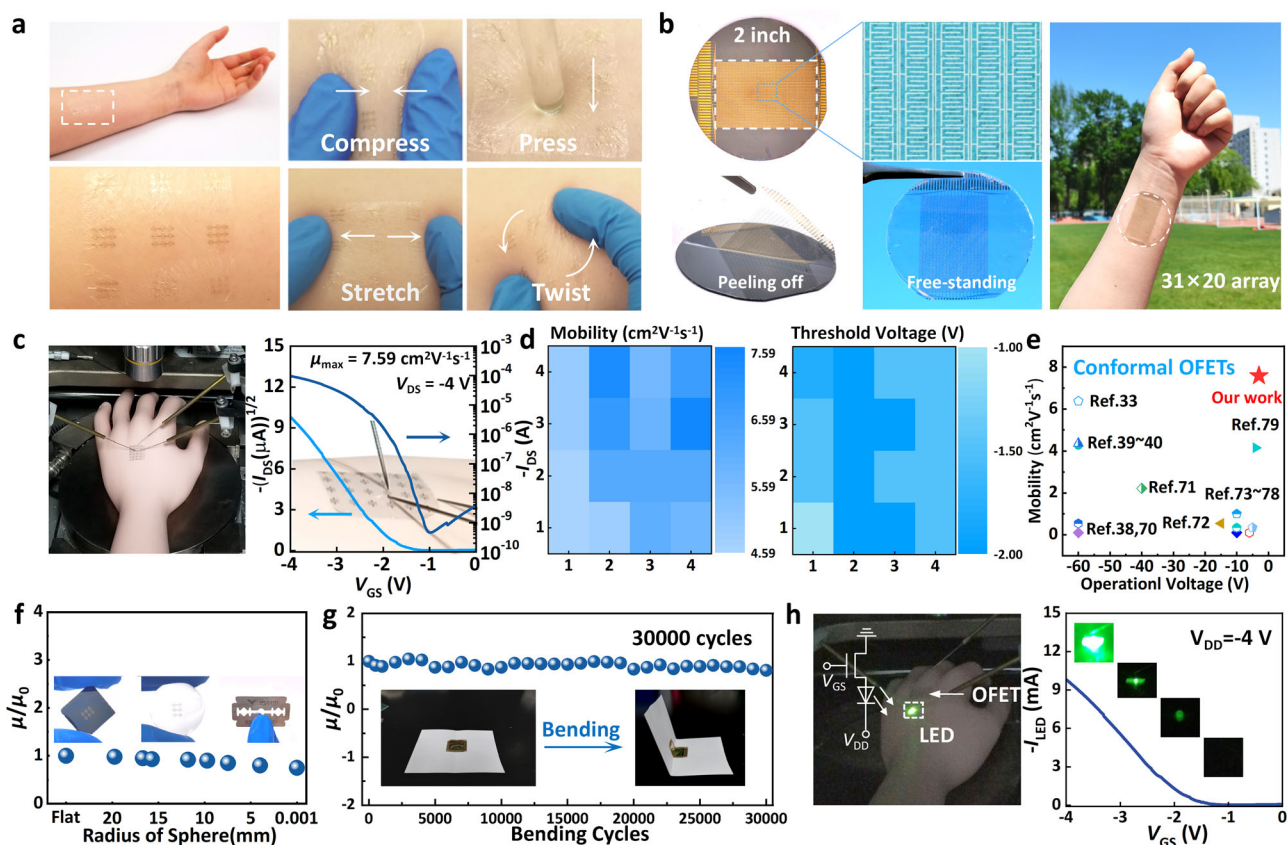
Fig. 6 | Conformability and electrical properties of low-voltage ultraflexible organic transistors. a Photographs of the transistor array adhered to human skin with the compress, stretch, press, and twist process. **b** Photolithography-compatible 2-inch transistors. **c** Testing photographs of 4 × 4 OTFT array conformed onto the artificial hand and the typical transfer curve. **d** Color mapping images of mobility and threshold voltage. **e** Statistical results of the mobilities and operational voltage of the reported conformal OFETs. **f** Normalize mobility of the conformal OFET with the bending radius from 20 mm to 1 μm. Inset are the typical photographs of transistors adhered on the flat Si substrate, 3D spherical surfaces, and the blade edge, respectively. **g** Normalize mobility of the ultraflexible transistor during 30,000 bending cycles. The bending was carried out on a standard 70 gsm printing paper with a bending radius of ~27 μm. **h** Driving ability of the conformal transistor for the modulated output current and LED lightness. Inset is the LED control circuit.

the chemical orthogonality with the photoresists[69]. Most of the commercial polymer dielectrics are easily dissolved or swelled in organic solvents, making it hard to compatible with photolithography process[5]. Here, benefiting from the excellent solvent resistance of QPSU dielectric, the photolithographic 31 × 20 organic transistor array can be fabricated on a 2-inch Si wafer, peeled and well adhered on human arm as shown in Fig. 6b. The peeled transistor array shows high transparency that can clearly see the blue sky and the photolithographic electrode patterns.

In Fig. 6c, d, a QPSU dielectric transistor array is attached to the back of an artificial hand without any bubbles, and all the conformal transistors can well work, with mobility as high as 7.59 cm² V⁻¹ s⁻¹, the threshold voltage as low as −1 V, and the operational voltage down to −4 V. Further, we compare the device performance with that of the reported conformal OFETs. As shown in Fig. 6e, our QPSU dielectric conformal device shows the highest mobility and lowest operational voltage[33,38–40,70–79] (Supplementary Table 6), showing the promising potential of our conformal transistors for future wearable electronics.

Further, to show the outstanding advantage of the ultrathin QPSU dielectric transistor in mechanical stability, the transistor was peeled from a flat Si substrate, and was respectively adhered onto the 3D spherical surfaces and the edge of the blade for comparison of performance. As shown in Fig. 6f, the device presents the normal operation with weak mobility changes at different bending spherical radius from 20 to 4 mm. Even at the bending radius as low as 0.001 mm at the edge of the blade, the mobility remains ~90% of the initial value. The transistor also presents good mechanical stability. As shown in Fig. 6g, when the transistor was adhered on the

printing paper and was folded with a bending radius of ~27 μm (Supplementary Fig. 19), the mobility changes weakly. Even after 30,000 bending cycles, the mobility remains 81% of the pristine mobility value.

As a typical example for future potential application, Fig. 6h shows the ultraflexible transistor adhered to the artificial hand that serves as the driver of a commercial organic light-emitting diode (OLED). With the changed gate voltage from −1 to −4 V, the OLED could be well controlled from the dark state to the lightened states with adjustable brightness. These results powerfully show the adherence capability of the QPSU dielectric OFETs, their driver capability in control circuits, and their outstanding advantages in safe operation and low-power consumption towards long-term imperceptible wearable electronics[80].

Discussion

In summary, we propose a novel method to simultaneously achieve low-voltage operation and high filed-effect mobility of the solution-processed ultraflexible organic transistor, by introducing a flexible quaternary ammonium side chain into PSU. The polar side chain is favorable to enhance the orientation polarization, and the methyl groups surrounding the nitrogen atom can produce the shielding effect to weaken the surface polarity. After the side chain incorporation in PSU, the operational voltage of organic transistor with QPSU dielectric decreases from −40 to −3 V, as a result of the increased dielectric constant from 3.9 to 18.8. The mobility is as high as 8.28 cm² V⁻¹ s⁻¹ at 1 Hz due to the weakened surface polarity by the increased methyl groups, which is the highest mobility of the reported C8-BTBT OFETs so far. The thickness of the fabricated QPSU dielectric OFET

can be as low as 135 nm, which is also in a class of the thinnest thickness of the reported OFETs. The mass is only ~0.5 g/m^2, which is about one order of magnitude lighter than that of a damselfly wing. The high transistor performance with low-voltage operation, high carrier mobility, good cyclic and long-term operation stability, combined with its ultrathin and ultralight characteristics, shows the promising potential of the QPSU dielectric transistor for the future low-power skin-like wearable electronics. Our results also open up a strategy for dielectric design of low-voltage, high-mobility organic transistor devices.

Methods

Materials
Polysulfone (PSU) (Mn = 80,000 g/mol) and C8-BTBT (>99% purity) were provided by Sigma Aldrich. Me0PSU, Me1PSU, Me2PSU, and Me3PSU (QPSU) were synthesized in our laboratory, and the synthesize routine is illustrated in the supplementary synthetic methods. PEDOT:PSS solution (Clevios PH1000) was purchased from Heraeus. Ethylene glycol (EG) and surface-active agent (Capstone FS-30) were purchased from Sigma Aldrich and DuPont, respectively. Chlorobenzene, acetone, and N,N-dimethylformamide were obtained from Beijing Chemical Reagent Co., Ltd. without further purification.

Fabrication of solution-processed QPSU dielectric OFETs
The Si substrate was cleaned in acetone and isopropanol by sonication for 10 min and subsequently dried by nitrogen. Then, the OTS treatment proceeded by dipping the Si wafers into OTS solution (OTS: heptane = 1:1000 by volume). Then, the PEDOT:PSS was spin-coated on the OTS-modified Si substrate at the spinning rate of 6000 rpm for 40 s and heated in the oven for 30 min to remove the residual water. The obtained PEDOT:PSS was dipped in the HNO$_3$ solution to improve the conductivity for 3 min and washed by deionized water. 1.28 g QPSU was dissolved in 17 mL N,N-Dimethylformamide with a solution concentration of 7 wt%. Then, the mixed solution of QPSU was stirred overnight to form uniform solution. The solution was spin-coated through a PVDF filter with a diameter of 0.2 μm on the PEDOT:PSS film. The QPSU thin film was placed in the 150 °C oven for 2 h to remove the residual solvent. After that, C8-BTBT was dissolved in chlorobenzene (5 mg/mL) at the spinning speeds from 6000 rpm for 40 s on the QPSU dielectric. Finally, 30 nm Au source and drain electrodes were thermally deposited by vacuum deposition (0.1 Å s^{-1}). The whole flexible polymer dielectric QPSU-based organic transistor was easily peeled off from Si wafer with the help of 3 M tape. The Me$_0$PSU, Me$_1$PSU and Me$_2$PSU dielectrics OFETs were also in the same device fabrication.

ESP of DFT calculation
The quantum chemical calculations were performed using the Gaussian 09 program package. Geometry optimizations for the molecules were modeled by the Density Function Theory (DFT) code B3LYP with the 6–31 G (d,p) basis set.

Lithography-compatibility 2-inch transistor
PEDOT:PSS solution was spin-coated on OTS/Si wafer and dipped in HNO$_3$ solution to improve its conductivity. After that, QPSU solution was spin-coated on PEDOT:PSS layer and placed in the 150 °C oven for 2 h to remove the residual solvent. Photoresist AZ5200NJ was spin-coated on QPSU dielectric and exposed to the 365 nm UV light. After that, the photoresist was developed in diluted AZ400K and evaporation Au electrode. Finally, the residual photoresist was removed by dissolving in acetone solution, and the C8-BTBT solution was spin-coated on the patterned Au electrode. The bottom-gate bottom-contact lithography 2-inch transistor was obtained.

Characterization
Optical microscopy investigation was performed with an Olympus BX51 microscope and a Keyence VHX-5000 (Keyence, Japan). AFM measurements were performed in the air with a Bruker Dimension Icon instrument (Bruker, Berlin, Germany). FTIR spectra were obtained by the Nicolet iS10 (Thermo Scientific). ^{1}H NMR spectra were obtained from Bruker Avance 500 MHz NMR and the deuterated dimethyl sulfoxide (DMSO-d$_6$) as the solvents. The capacitance of QPSU dielectric was measured by the IM3590 chemical impedance analyzer (Hioki Electric Co., Ltd) from 1 Hz to 200 KHz. The out-of-plane and in-plane grazing incidence X-ray diffraction (GIXRD) was conducted on Rigaku Smart Lab with Cu Kα source (λ = 1.54056 Å) in air.

The electrical characteristics of OFET devices were recorded with a Keithley 4200 SCS and a Cascade M150 probe station at room temperature in the air. All the field-effect parameters are calculated with the standard equation in the saturation regime. The standard equation is

$$I_{GS} = \frac{\mu W C_i}{2L} \left(V_G - V_T \right)^2 \tag{1}$$

Where W ($W = 100$ μm) and L ($L = 3500$ μm) are the channel width and channel length, respectively. C_i is the capacitance per unit area of QPSU, which is 185 nF/cm^2 at 1 Hz, I_{DS} is the drain current, and V_{GS} is the gate voltage. The transfer curves of the QPSU dielectric were measured within 2 seconds, which is consistent with the frequency of the dielectric capacitance, leading to highly reliable mobility results.

Data availability
Additional data related to this paper may be requested from the corresponding authors upon reasonable request.

References
1. Arias, A. C., MacKenzie, J. D., McCulloch, I., Rivnay, J. & Salleo, A. Materials and applications for large area electronics: solution-based approaches. *Chem. Rev.* **110**, 3–24 (2010).
2. Kaltenbrunner, M. et al. An ultra-lightweight design for imperceptible plastic electronics. *Nature* **499**, 458–463 (2013).
3. Zhang, X. et al. Alignment and patterning of ordered small-molecule organic semiconductor micro/nanocrystals for device applications. *Adv. Mater.* **28**, 2475–2503 (2016).
4. Liu, X. et al. Epitaxial ultrathin organic crystals on graphene for high-efficiency phototransistors. *Adv. Mater.* **28**, 5200–5205 (2016).
5. Wang, S. et al. Skin electronics from scalable fabrication of an intrinsically stretchable transistor array. *Nature* **555**, 83–88 (2018).
6. Kwon, J. et al. Three-dimensional monolithic integration in flexible printed organic transistors. *Nat. Commun.* **10**, 54 (2019).
7. Duan, S. et al. Solution-processed centimeter-scale highly aligned organic crystalline arrays for high-performance organic field-effect transistors. *Adv. Mater.* **32**, 1908388 (2020).
8. Sirringhaus, H. 25th anniversary article: organic field-effect transistors: the path beyond amorphous silicon. *Adv. Mater.* **26**, 1319–1335 (2014).
9. Troisi, A. Charge transport in high mobility molecular semiconductors: classical models and new theories. *Chem. Soc. Rev.* **40**, 2347–2358 (2011).
10. Diao, Y. et al. Solution coating of large-area organic semiconductor thin films with aligned single-crystalline domains. *Nat. Mater.* **12**, 665–671 (2013).
11. Nketia-Yawson, B. & Noh, Y. Y. Recent progress on high-capacitance polymer gate dielectrics for flexible low-voltage transistors. *Adv. Funct. Mater.* **28**, 1802201 (2018).
12. Zhang, M. et al. Dielectric design of high dielectric constant poly (urea-urethane) elastomer for low-voltage high-mobility intrinsically stretchable all-solution-processed organic transistors. *Small*, **2311527**, https://doi.org/10.1002/smll.202311527 (2024).

13. Rahmanudin, A. et al. Robust high-capacitance polymer gate dielectrics for stable low-voltage organic field-effect transistor sensors. *Adv. Electron. Mater.* **6**, 1901127 (2020).

14. Haase, K. et al. Solution shearing of a high-capacitance polymer dielectric for low-voltage organic transistors. *Adv. Electron. Mater.* **5**, 1900067 (2019).

15. Roberts, M. E. et al. Cross-linked polymer gate dielectric films for low-voltage organic transistors. *Chem. Mater.* **21**, 2292–2299 (2009).

16. Jeong, S., Kim, D. & Moon, J. Ink-Jet-printed organic-inorganic hybrid dielectrics for organic thin-film transistors. *J. Phys. Chem. C.* **112**, 5245–5249 (2008).

17. Kaihovirta, N., Aarnio, H., Wikman, C. J., Wilén, C. E. & Österbacka, R. The effects of moisture in low-voltage organic field-effect transistors gated with a hydrous solid electrolyte. *Adv. Funct. Mater.* **20**, 2605–2610 (2010).

18. von Seggern, F. et al. Temperature-dependent performance of printed field-effect transistors with solid polymer electrolyte gating. *ACS Appl. Mater. Interfaces* **8**, 31757–31763 (2016).

19. Naber, R. C. et al. High-performance solution-processed polymer ferroelectric field-effect transistors. *Nat. Mater.* **4**, 243–248 (2005).

20. Kim, J. O. et al. Network structure modification-enabled hybrid polymer dielectric film with zirconia for the stretchable transistor applications. *Adv. Funct. Mater.* **30**, 1906647 (2020).

21. Kim, S. H. et al. Electrolyte-gated transistors for organic and printed electronics. *Adv. Mater.* **25**, 1822–1846 (2013).

22. Rahimabady, M. et al. Intermolecular interactions and high dielectric energy storage density in poly (vinylidene fluoride-hexafluoropropylene)/poly (vinylidene fluoride) blend thin films. *Appl. Phys. Lett.* **100**, 25 (2012).

23. Ye, H. et al. The hidden potential of polysilsesquioxane for high-k: analysis of the origin of its dielectric nature and practical low-voltage-operating applications beyond the unit device. *Adv. Funct. Mater.* **32**, 2104030 (2022).

24. Wang, B. et al. High-k gate dielectrics for emerging flexible and stretchable electronics. *Chem. Rev.* **118**, 5690–5754 (2018).

25. Zheng, W. et al. Temperature resistant amorphous polyimides with high intrinsic permittivity for electronic applications. *Chem. Eng. J.* **436**, 135060 (2022).

26. Zhu, Y.-F., Zhang, Z., Litt, M. H. & Zhu, L. High dielectric constant sulfonyl-containing dipolar glass polymers with enhanced orientational polarization. *Macromolecules* **51**, 6257–6266 (2018).

27. Chong, K., Lai, S., Thiam, H., Teoh, H. & Heng, S. Recent progress of oxygen/nitrogen separation using membrane technology. *J. Eng. Sci. Technol.* **11**, 1016–1030 (2016).

28. Hiemenz, P. C. & Lodge, T. P. Polymer chemistry. (CRC Press, 2007).

29. Ye, H. et al. Photopatternable high-k polysilsesquioxane dielectrics for organic integrated devices: effects of UV curing on chemical and electrical properties. *Adv. Funct. Mater.* **33**, 2214865 (2023).

30. Miao et al. Quaternized polyhedral oligomeric silsesquioxanes (QPOSS) modified polysulfone-based composite anion exchange membranes. *Solid State Ion.* **309**, 170–179 (2017).

31. Liu, Z., Yin, Z., Wang, J. & Zheng, Q. Polyelectrolyte dielectrics for flexible low-voltage organic thin-film transistors in highly sensitive pressure sensing. *Adv. Funct. Mater.* **29**, 1806092 (2019).

32. Lee, J. et al. Ion gel-gated polymer thin-film transistors: operating mechanism and characterization of gate dielectric capacitance, switching speed, and stability. *J. Phys. Chem. C.* **113**, 8972–8981 (2009).

33. Zhang, M. et al. Highly stable nonhydroxyl antisolvent polymer dielectric: a new strategy towards high-performance low-temperature solution-processed ultraflexible organic transistors for skin-inspired electronics. *Research* **2021**, 9897353 (2021).

34. Altun, V., Remigy, J.-C. & Vankelecom, I. F. UV-cured polysulfone-based membranes: effect of co-solvent addition and evaporation process on membrane morphology and SRNF performance. *J. Membr. Sci.* **524**, 729–737 (2017).

35. Yang, N., Liang, Y. & Jia, S. Enhanced thermal stability and electrochemical performance of polyacrylonitrile/cellulose acetate-electrospun fiber membrane by boehmite nanoparticles: application to high-performance lithium-ion batteries. *Macromol. Mater. Eng.* **306**, 2100300 (2021).

36. Panidi, J. et al. Remarkable enhancement of the hole mobility in several organic small-molecules, polymers, and small-molecule: polymer blend transistors by simple admixing of the Lewis acid P-dopant B (C6F5) 3. *Adv. Sci.* **5**, 1700290 (2018).

37. Cui, N. et al. Fully transparent conformal organic thin-film transistor array and its application as LED front driving. *Nanoscale* **10**, 3613–3620 (2018).

38. Liu, M. et al. Ultrathin free-substrate n-type PTCDI-C13 transistors with bilayer polymer dielectrics. *IEEE Trans. Electron Devices* **39**, 1183–1186 (2018).

39. Ren, H. et al. High-performance, ultrathin, ultraflexible organic thin-film transistor array via solution process. *Small* **14**, 1801020 (2018).

40. Ren, H., Tang, Q., Tong, Y. & Liu, Y. 320-nm flexible solution-processed 2, 7-dioctyl [1] benzothieno [3, 2-b] benzothiophene transistors. *Materials* **10**, 918 (2017).

41. Chen, X. et al. Low-power flexible organic field-effect transistors with solution-processable polymer-ceramic nanoparticle composite dielectrics. *Nanomaterials* **10**, 518 (2020).

42. Zhao, W. et al. A facile method for the growth of organic semiconductor single crystal arrays on polymer dielectric toward flexible field-effect transistors. *Adv. Funct. Mater.* **29**, 1902494 (2019).

43. Sung, S. et al. Large-area printed low-voltage organic thin film transistors via minimal-solution bar-coating. *J. Mater. Chem. C.* **8**, 15112–15118 (2020).

44. Shin, E. Y., Cho, H. J., Jung, S., Yang, C. & Noh, Y. Y. A high-k fluorinated P (VDF-TrFE)-g-PMMA gate dielectric for high-performance flexible field-effect transistors. *Adv. Funct. Mater.* **28**, 1704780 (2018).

45. Ji, D. et al. Surface polarity and self-structured nanogrooves collaboratively oriented molecular packing for high crystallinity toward efficient charge transport. *J. Am. Chem. Soc.* **139**, 2734–2740 (2017).

46. Ji, D. et al. Copolymer dielectrics with balanced chain-packing density and surface polarity for high-performance flexible organic electronics. *Nat. Commun.* **9**, 2339 (2018).

47. Ji, D. et al. Highly efficient charge transport in a quasi-monolayer semiconductor on pure polymer dielectric. *Adv. Funct. Mater.* **30**, 1907153 (2020).

48. Wang, W. et al. Neuromorphic sensorimotor loop embodied by monolithically integrated, low-voltage, soft e-skin. *Science* **380**, 735–742 (2023).

49. Gelinck, G. H. et al. Flexible active-matrix displays and shift registers based on solution-processed organic transistors. *Nat. Mater.* **3**, 106–110 (2004).

50. Klauk, H., Zschieschang, U., Pflaum, J. & Halik, M. Ultralow-power organic complementary circuits. *Nature* **445**, 745–748 (2007).

51. Richards, T., Bird, M. & Sirringhaus, H. A quantitative analytical model for static dipolar disorder broadening of the density of states at organic heterointerfaces. *J. Chem. Phys.* **128**, 234905 (2008).

52. Kong, D. et al. Capacitance characterization of elastomeric dielectrics for applications in intrinsically stretchable thin film transistors. *Adv. Funct. Mater.* **26**, 4680–4686 (2016).

53. Zhuang, X. et al. Frequency-agile low-temperature solution-processed alumina dielectrics for inorganic and organic electronics enhanced by fluoride doping. *J. Am. Chem. Soc.* **142**, 12440–12452 (2020).

54. Choi, J., Kang, J., Lee, C., Jeong, K. & Im, S. G. Heavily crosslinked, high-k ultrathin polymer dielectrics for flexible, low-power organic thin-film transistors (OTFTs). *Adv. Electron. Mater.* **6**, 2000314 (2020).

55. Chen, H. et al. Highly efficient flexible organic light emitting transistor based on high-K polymer gate dielectric. *Adv. Opt. Mater.* **8**, 1901651 (2020).

56. Cao, J. et al. Polysiloxane–poly (vinyl alcohol) composite dielectrics for high-efficiency low voltage organic thin film transistors. *J. Mater. Chem. C.* **7**, 4879–4886 (2019).

57. Dai, S. et al. Intrinsically ionic conductive cellulose nanopapers applied as all solid dielectrics for low voltage organic transistors. *Nat. Commun.* **9**, 2737 (2018).

58. Lei, Y., Wu, B., Chan, W.-K. E., Zhu, F. & Ong, B. S. Engineering gate dielectric surface properties for enhanced polymer field-effect transistor performance. *J. Mater. Chem. C.* **3**, 12267–12272 (2015).

59. Lei, Y. et al. Enhancing crystalline structural orders of polymer semiconductors for efficient charge transport via polymer-matrix-mediated molecular self-assembly. *Adv. Mater.* **28**, 6687–6694 (2016).

60. Deng, W. et al. Scalable growth of organic single-crystal films via an orientation filter funnel for high-performance transistors with excellent uniformity. *Adv. Mater.* **34**, 2109818 (2022).

61. Xu, K. et al. Sub-10 nm nanopattern architecture for 2D material field-effect transistors. *Nano. Lett.* **17**, 1065–1070 (2017).

62. Minemawari, H. et al. Inkjet printing of single-crystal films. *Nature* **475**, 364–367 (2011).

63. Takimiya, K., Osaka, I., Mori, T. & Nakano, M. Organic semiconductors based on [1] benzothieno [3, 2-b][1] benzothiophene substructure. *Acc. Chem. Res.* **47**, 1493–1502 (2014).

64. Ebata, H. et al. Highly soluble [1] benzothieno [3, 2-b] benzothiophene (BTBT) derivatives for high-performance, solution-processed organic field-effect transistors. *J. Am. Chem. Soc.* **129**, 15732–15733 (2007).

65. Izawa, T., Miyazaki, E. & Takimiya, K. Molecular ordering of high-performance soluble molecular semiconductors and re-evaluation of their field-effect transistor characteristics. *Adv. Mater.* **20**, 3388–3392 (2008).

66. Kwon, S. et al. Organic single-crystal semiconductor films on a millimeter domain scale. *Adv. Mater.* **27**, 6870–6877 (2015).

67. Fan, X., Wu, Z., Wang, L. & Wang, C. Exploring the origin of high dechlorination activity in polar materials M2B5O9Cl (M= Ca, Sr, Ba, Pb) with built-in electric field. *Chem. Mater.* **29**, 639–647 (2017).

68. Zhou, S. et al. Direct effect of dielectric surface energy on carrier transport in organic field-effect transistors. *ACS Appl. Mater. Interfaces* **10**, 15943–15951 (2018).

69. Zheng, Y.-Q. et al. Monolithic optical microlithography of high-density elastic circuits. *Science* **373**, 88–94 (2021).

70. Cosseddu, P., Piras, A. & Bonfiglio, A. Fully deformable organic thin-film transistors with moderate operation voltage. *IEEE Trans. Electron Devices* **58**, 3416–3421 (2011).

71. Zhou, Y. et al. Solution-processed single-crystal array for high-performance conformable transistors. *IEEE Electron Device* **39**, 595–598 (2018).

72. Zhang, L. et al. Substrate-free ultra-flexible organic field-effect transistors and five-stage ring oscillators. *Adv. Mater.* **25**, 5455–5460 (2013).

73. Fukuda, K. et al. Fully-printed high-performance organic thin-film transistors and circuitry on one-micron-thick polymer films. *Nat. Commun.* **5**, 4147 (2014).

74. Takeda, Y. et al. Fabrication of ultra-thin printed organic TFT CMOS logic circuits optimized for low-voltage wearable sensor applications. *Sci. Rep.* **6**, 25714 (2016).

75. Fukuda, K. et al. Free-standing organic transistors and circuits with sub-micron thicknesses. *Sci. Rep.* **6**, 27450 (2016).

76. Stucchi, E., Scaccabarozzi, A. D., Viola, F. A. & Caironi, M. Ultraflexible all-organic complementary transistors and inverters based on printed polymers. *J. Mater. Chem. C.* **8**, 15331–15338 (2020).

77. Viola, F. A. et al. A sub-150-nanometre-thick and ultraconformable solution-processed all-organic transistor. *Nat. Commun.* **12**, 5842 (2021).

78. Nawrocki, R. A., Matsuhisa, N., Yokota, T. & Someya, T. 300-nm imperceptible, ultraflexible, and biocompatible e-skin fit with tactile sensors and organic transistors. *Adv. Electron. Mater.* **2**, 1500452 (2016).

79. Ji, X. et al. Smart surgical catheter for C-reactive protein sensing based on an imperceptible organic transistor. *Adv. Sci.* **5**, 1701053 (2018).

80. Wu, Z. et al. Efficient and low-voltage vertical organic permeable base light-emitting transistors. *Nat. Mater.* **20**, 1007–1014 (2021).

Author contributions
M. Zhang, Y. Tong, X. Zhao, Q. Tang, and Y. Liu conceived the research topic. M. Zhang conducted the experiments. X. Wang conducted the theoretical analyses. C. Zhang, H. Yu, and S. Guo helped to modify the diagram. J. Sun took photos of the flexible organic transistors. All authors analyzed the data and discussed the results.

Competing interests
The authors declare no competing interests.

Additional information
Supplementary information The online version contains supplementary material available at https://doi.org/10.1038/s41528-024-00316-0.

Correspondence and requests for materials should be addressed to Yanhong Tong or Qingxin Tang.

Reprints and permissions information is available at http://www.nature.com/reprints

Publisher's note Springer Nature remains neutral with regard to jurisdictional claims in published maps and institutional affiliations.